# Modeling Energy Harvesting From Membrane Vibrations using Multi-physics Modeling

Raymond C. Singh

Thesis submitted to the Faculty of

Virginia Polytechnic Institute and State University

in partial fulfillment of the requirements for the degree of

Master of Science

in

Aerospace Engineering

Rakesh K. Kapania, Chair

Cornel Sultan

Michael K. Philen

April 30, 2012

Blacksburg, Virginia

Keywords: Piezoelectric, Energy Harvesting, Membranes, Computational Methods

# Modeling Energy Harvesting From Membrane Vibrations using Multi-physics Modeling

Raymond C. Singh

## ABSTRACT

Given the ever-growing need for device autonomy and renewable sources of energy, energy harvesting has become an increasingly popular field of research. This research focuses on energy harvesting using the piezoelectric effect, from vibrating membrane structures by converting mechanical energy into electric energy. Specific applications of this research include powering components of bio-inspired micro air vehicles (MAVs), which require long range with as little regular maintenance as possible, and powering sensors for structural health monitoring on otherwise inaccessible locations (the roof of the Denver Int'l Airport is a good example). Coming up with an efficient, high-fidelity model of these systems allows for design optimization without the extensive use of experimental testing, as well as a deeper understanding of the physics involved. These are the twin goals of this research. This work describes a modeling algorithm using COMSOL, a multi-physics software, to predict the structural mechanics of and subsequent power harvested from a piezoelectric patch placed on a prestressed membrane structure. The model is verified by an FE comparison of the modeled system's dynamic response. For a 0.5 x 0.5 x 0.001 m nylon membrane with a 0.1 x 0.1 x 0.001 m piezoelectric patch placed on its corner, a maximum power output of ~10 microwatts was achieved, using a resistance of 100 Ohms and exciting the system around resonance. When the patch was placed on the side of the membrane, the power output was ~100 milliwatts. The ultimate goal is to estimate the energy harvested by a network of these piezoelectric patches and optimize the harvesting system based on the size, shape and location of the patches.

Dedication

This work is dedicated to my God, my family, my friends and all those who have helped and encouraged me to overcome adversity in order to pursue my passion for engineering.

Acknowledgments

I would like to thank first and foremost my advisors, Dr. Rakesh Kapania and Dr. Cornel Sultan for their valuable guidance and boundless patience. I would also like to thank Dr. Michel Philen and Dr. Mohammed Sunny for aiding this research work with their knowledge and support. Lastly, I thank the Institute for Critical Technologies and Applied Sciences (ICTAS @ VT) as well as the Virginia Tech Space Grant Consortium for funding this research.

# Table Of Contents

# List of Figures

# List of Tables

# Nomenclature

| | |
|---|---|
| $C_p^S$ | internal capacitance of the piezoelectric material |
| d | piezoelectric strain coefficient |
| D | electric displacement |
| E | electric field |
| ε | dielectric permittivity |
| $F_0$ | pressure amplitude |
| I | current |
| L | inductance |
| mg | acceleration due to gravity |
| P | power harvested |
| q | charge |
| R | resistance |
| s | mechanical compliance |
| S | strain |
| T | stress |
| U | energy |
| V | electric potential |
| w | vertical displacement |
| $\omega_0$ | excitation frequency |
| $\omega_n$ | natural frequency |

Chapter 1

# Introduction

Modeling piezoelectric energy harvesting from prestressed, thin-film membrane structures is a more novel and complex problem than what has been explored previously. Capturing the change in stiffness from the prestress, the electromechanical coupling between the substrate and the piezoelectric patch, and the interaction between the structural system and the energy dissipation resulting from the harvesting process are a few of the challenges in accurately and efficiently predicting the overall response of the structure. This section will outline the physics of piezoelectric materials as a foundation for the following discussion, provide a review of the efforts made in the modeling and testing of piezoelectric energy harvesting devices, summarize previous studies on vibrating membrane structures, and detail potential applications for the technologies modeled. It also states the objectives of the research, as well as the approach taken to solve the research problem.

## 1.1 Background on Piezoelectric Materials

All piezoelectric materials have inherent electromechanical coupling, meaning that a mechanical stress will produce an electric displacement, while an electric field will incite mechanical

strain. The former is called the direct piezoelectric effect, while the latter is the converse piezoelectric effect. This coupling is due to the presence of electric dipoles in the material. For instance, a piezoelectric sample may have a certain polarization vector when unstressed. When a strain is applied, the particles shift, causing the polarization vector to change, inducing an electric potential at the electrodes of the sample. Now, in addition to the typical stress-strain relationship, there is electromechanical coupling. The net charge flow divided by the area of the electrodes is the electric displacement D, and is related to the stress T by the piezoelectric strain coefficient d, while in the elastic regime.

$$D = d\,T \tag{1}$$

Similarly, for purely electrical studies, the electric displacement D is equal to the electric field E multiplied by the dielectric permittivity ε

$$D = \epsilon E \tag{2}$$

and the strain S is related to the electric field by the piezoelectric strain coefficient d

$$S = dE \tag{3}$$

In matrix form, the constitutive relationships would be

$$\begin{bmatrix} S \\ D \end{bmatrix} = \begin{bmatrix} s & d \\ d & \epsilon \end{bmatrix} \begin{bmatrix} T \\ E \end{bmatrix} \tag{4}$$

In general, for a 3-D piezoelectric cube,

$$E = \begin{bmatrix} E_1 \\ E_2 \\ E_3 \end{bmatrix}, D = \begin{bmatrix} D_1 \\ D_2 \\ D_3 \end{bmatrix} \tag{5}$$

and in indicial notation,

$$D_m = \epsilon'_{mn} * E_n \tag{6}$$

For stress-strain, note that there are 3 normal components and 6 shear components, so the compliance tensor will have 81 terms:

$$S_{ij} = s_{ijkl} * T_{kl} \tag{7}$$

Finally, the coupling relations are

$$S_{ij} = d_{ijn} * E_n \tag{8}$$

$$D_m = d_{mkl} * T_{kl} \tag{9}$$

and combining, we get the complete constitutive equations for a linear piezoelectric material:

$$S_{ij} = s_{ijkl} * T_{kl} + d_{ijn} * E_n \tag{10}$$

$$D_m = d_{mkl} * T_{kl} + \epsilon'_{mn} * E_n \tag{11}$$

In compact notation, $T_{ij} = T_{ji}$, $T_{ii} = T_i$, due to symmetry. Similarly, $S_{ii} = S_i$ and

$$S_i = s_{ij} * T_j + d_{ik} * E_k \tag{12}$$

$$D_m = d_{mj} * T_j + \epsilon'_{mk} * E_n \tag{13}$$

Expanding,

$$\begin{bmatrix} S_1 \\ S_2 \\ S_3 \\ S_4 \\ S_5 \\ S_6 \end{bmatrix} = \begin{bmatrix} s_{11} & s_{12} & s_{13} & s_{14} & s_{15} & s_{16} \\ s_{21} & s_{22} & s_{23} & s_{24} & s_{25} & s_{26} \\ s_{31} & s_{32} & s_{33} & s_{34} & s_{35} & s_{36} \\ s_{41} & s_{42} & s_{43} & s_{44} & s_{45} & s_{46} \\ s_{51} & s_{52} & s_{53} & s_{54} & s_{55} & s_{56} \\ s_{61} & s_{62} & s_{63} & s_{64} & s_{65} & s_{66} \end{bmatrix} \begin{bmatrix} T_1 \\ T_2 \\ T_3 \\ T_4 \\ T_5 \\ T_6 \end{bmatrix} + \begin{bmatrix} d_{11} & d_{12} & d_{13} \\ d_{21} & d_{22} & d_{23} \\ d_{31} & d_{32} & d_{33} \\ d_{41} & d_{42} & d_{43} \\ d_{51} & d_{52} & d_{53} \\ d_{61} & d_{62} & d_{63} \end{bmatrix} \begin{bmatrix} E_1 \\ E_2 \\ E_3 \end{bmatrix} \tag{14}$$

Most piezoelectric elements can be modeled as orthotropic materials, simplifying the compliance matrix to [1]

$$s^E = \begin{bmatrix} 1/Y_1^E & -\nu_{12}/Y_1^E & -\nu_{13}/Y_1^E & 0 & 0 & 0 \\ -\nu_{21}/Y_2^E & 1/Y_2^E & -\nu_{23}/Y_2^E & 0 & 0 & 0 \\ -\nu_{31}/Y_3^E & -\nu_{32}/Y_3^E & 1/Y_3^E & 0 & 0 & 0 \\ 0 & 0 & 0 & 1/G_{23}^E & 0 & 0 \\ 0 & 0 & 0 & 0 & 1/G_{13}^E & 0 \\ 0 & 0 & 0 & 0 & 0 & 1/G_{12}^E \end{bmatrix} \tag{15}$$

Since electric fields applied in a certain direction will not produce electric displacements in orthogonal directions,

$$\epsilon = diag(\epsilon) \tag{16}$$

and the strain coefficient matrix becomes

$$d = \begin{bmatrix} 0 & 0 & 0 & 0 & d_{15} & 0 \\ 0 & 0 & 0 & d_{24} & 0 & 0 \\ d_{13} & d_{23} & d_{33} & 0 & 0 & 0 \end{bmatrix} \tag{17}$$

These properties are generally available from vendors. The indices 33 and 31 in the coefficient matrix correspond to the two most common operating modes for a piezoelectric device. The 33 mode (if the 3-direction is in the direction of polarization; for a typical PZT, this is through the thickness) is where the polarization changes for stresses in the 3 direction. The 33 mode is generally more efficient in transducing mechanical energy to electrical and vice versa, and is seen in stack actuators. The 31 mode applies an electric field in the 3 direction but uses the stresses induced in the 1 (extensional in-plane) direction for bending or extension. This is the mode typically used in bimorph bending and plate/membrane devices. Given an operating mode, these constitutive relationships define the material, and can be used to derive the governing equations of motion for a piezoelectric system [1].

## 1.2 Piezoelectric Energy Harvesting

Experimental investigations into the merit of piezoelectric energy harvesting have more recently been motivated by the demand for increased autonomy, portability, and lifespan of wireless devices. Sensor networks, for instance, may be placed in remote areas, in which case conducting regular maintenance such as replacing and recharging a power source is costly and inefficient. The energy density of batteries, despite considerable progress, has still not increased to a level that will meet the capabilities of the devices that utilize them. Harvesting ambient energy has a large amount of potential to alleviate these issues. Anton and Sodano [2] presented an exhaustive review of the current technology base for energy harvesting, specifically focusing on piezoelectric vibrational harvesting. However, there are several other sources from which ambient energy can be utilized, e.g. electromagnetic waves, fluid flow, and solar energy. For the purposes of this research, a survey of vibrational harvesting techniques was conducted.

Anton and Sodano also compiled a summary of the various piezoelectric materials usually used for harvesting applications. The most common material is the piezoceramic (PZT), which has superior electromechanical coupling, but has the disadvantage of being quite brittle. Electroactive polymers such as polyvinylidene fluoride (PVDF) do have the ability to support large strains, but unlike the PZT ceramic, have low coupling properties. Martin [3] analyzed the potential of ionic electroactive polymers as energy harvesting devices used to power wireless sensors. After mathematically deriving the transfer functions for open-circuit voltage and closed-circuit current, the theoretical maximum power was evaluated alongside experimental testing. It was found that the transducer could not produce an adequate amount of power, but did show promise as an energy storage device. Attempts at compromising flexibility and electromechanical coupling have been documented, as well. Piezofiber composites such as the Quick Pack IDE (inter-digitated electrodes) and Smart Material's MFC (macro-fiber composite) embed piezoceramic fibers in a flexible laminate matrix. Sodano et al. [4] compared the power generation capabilities of the MFC, Quick Pack (PZT ceramic) and Quick Pack IDE. Using a cantilever beam setup excited with base motion from a shaker at various resonant beam frequencies, both maximum instantaneous power and average power normalized by the volume of the materials were measured. It was found that the Quick Pack had the highest power generation; the Quick Pack IDE had equivalent generating capabilities to the MFC. The work noted that the interdigitation lead to low capacitance versus a d33 Quick Pack, which is a direct "parallel-plate" style dielectric medium. Yang et al. [5] developed and modeled an energy harvesting system utilizing three MFC patches on a cantilever beam in an optimized configuration. For excitation around the first resonant frequency, the maximum power was 151.6 μW.

In addition to material selection, changes in configuration of electrodes (33 vs. 31 direction, number of electrodes), the number of piezoelectric layers (unimorph vs. bimorph), geometries for both the substrate as well as the piezoelectric devices themselves, and circuitry/energy storage methods have

also been studied. Kim et al. [6] designed a cymbal-shaped transducer to work under high-impact, low-frequency conditions. For a force of 70 N at a frequency of 100 Hz directly applied in the 33 direction, the generator (diameter = 29 mm, t = 1.8 mm) produced 52 mW of power across a 400 kΩ resistor. For more plate and membrane-oriented applications, Minazara et al. [7] designed an energy harvesting generator using a piezoelectric unimorph diaphragm. The paper reported a maximum power of 1.7 mW for a transverse force of 80 N (excited via a shaker) and a load resistance of 47 kΩ.

Harvesting energy from stray electromagnetic fields is also undergoing significant development. Beeby, et al. [8] proposed an electromagnetic generator optimized for low ambient vibrations. The design consisted of a cantilever beam with a set of magnets, coil and a tungsten tip mass at the free end. It produced 46 μW from an excitation of 0.59 $m/s^2$ (60 *mg*) near the first resonance frequency (52 Hz) and a load resistance of 4 kΩ. A survey of electromagnetic harvesters in the same work showed that the technology has a better power density as compared to piezoelectric devices. Dong et al. [9] investigated a design that simultaneously harvested energy from magnetic fields and vibrations. The multi-modal system consisted of a cantilever beam with a tip mass and a magnetoelectric laminate attached in the center of the beam. At 2 Oe (1 Oersted = 1000/4π A/m) field strength and vibration amplitude of 50 *mg* at 20 Hz, the open-circuit voltage was found to be 8 V. The design demonstrated the capability of energy harvesting devices to utilize more than one energy source and thus achieve a higher power density.

## 1.3 Modeling of Piezoelectric Energy Harvesting

As evidenced above, efforts have been made to design efficient piezoelectric transducers, but the majority of the research in this emerging market has been devoted to understanding and modeling the piezoelectric harvesting process. Sodano, Park and Inman [10] developed an analytical model for a bimorph PZT harvester in a cantilever beam configuration. Equations of motion for the system were

derived from Hamilton's principle and strain energy methods. The dissipation due to the harvester circuit was applied as an electrical BC $V = -R\dot{q}(t)$; structural damping was also taken into consideration. The approach was validated by testing a Quick Pack ceramic beam excited by a shaker. The current output was accurately predicted by the model; for a harmonic input, the power output will not die out. Closed-form analytical formulations were presented in a paper by Erturk and Inman [11]; an exact solution for the power output of a cantilevered piezoelectric energy harvester due to base motion was found. Starting with the constitutive equations, the electric displacement, and thus the charge and current, was derived. The model was tested on a unimorph and successfully predicted the response. Khameneifar et al. [12] modeled a piezo beam mounted on a rotating hub to simulate harvesting under rotary motion. Again, the equations of motion were derived with a Lagrangian approach, producing numerical results relating the hub motion to the power harvested.

The dissipation in the structural response caused by the harvesting circuit is analogous to piezoelectric shunt damping, a subject for which significant work has been published. Hagood and von Flotow [13] derived effective impedances for a piezoelectric device shunted by passive circuitry (either a resistor or a resistor-inductor), and analyzed a cantilever beam experiment equipped with two bimorphs for energy dissipation. The method was validated by experimental data, and it was found that the RL circuit could be tuned to resonance like the classical vibration absorber. Corr and Clark [14] tested two shunt damping techniques and compared them to the passive resonant shunt circuit examined in [13]. Along the way, they derived the transducer equations and equations of motion for a 1-D stack actuator, and subsequently modeled the energy dissipation. The piezoelectric material was modeled as an AC voltage source:

$$V_a = -\frac{k_s^E d_{33} y(t)}{C_p^S} \tag{18}$$

in series with the internal capacitance $C_p^S$, and was then connected to the resonant shunt RL. The circuit equations were calculated in terms of the applied charge $Q_{app}$, then the entire system of

governing equations was converted to the Laplace domain from the time domain to get the response with damping included, dissipating energy as $I^2R$ over the entire vibration cycle. The energy loss factor over one cycle of harmonic displacement/radian:

$$\eta = \frac{k_{33}^2 \omega_0^2 \omega_n RL}{\left(\omega_0^2 - \omega_n^2\right)^2 + \left(\omega_n\left(\frac{R}{L}\right)\right)^2 - k_{33}^2 \omega_0^2 (\omega_0^2 - \omega_n^2)} \tag{19}$$

where $\omega_0$ is the optimal tuning frequency $\sqrt{\frac{1}{LC_p^S}}$.

Far less work has been conducted on the modeling of piezoelectric patches on plates and membranes, however. Kim et al. [15] explored piezoelectric plate theory by modeling clamped unimorph PZT plates. For varying design parameters such as thickness, the energy harvested could be calculated; the equations for current, voltage and capacitance were derived from constitutive relations and energy expressions, upon which $U_{gen} = 0.5CV_{gen}^2$. Switching from analytical to finite element methods, Taleghani [16] used NASTRAN/ANSYS to precisely predict the displacements in NASA's THUNDER (THin layer UNimorph ferroelectric DrivER) patches due to an actuation voltage.

Computational methods have been employed to increase the ease of analyzing complex piezoelectric systems with interaction between multiple domains of physics. Elvin and Elvin [17] engineered a coupled FEM-SPICE model for analyzing piezoelectric energy generators. In their algorithm, the FEM code takes the mechanical system and generates a voltage response, the Simulation Program with Integrated Circuit Emphasis (SPICE) code solves the generator circuit model and outputs the voltage at the next time step, the voltage is then fed back into the FEM code, and this process is iterated for the entirety of the sampled response. The unimorph cantilever subject from [11] was used for validation and comparison, and the frequency response functions for the power and voltage were comparable. The multiphysics package COMSOL has been successfully used to generate predictions of the system response for a piezoelectric structure. Emam [18] modeled a composite cantilever PZT beam using various analyses and materials. A static test was first conducted to figure out the maximum

strain due to a tip load. Following that was a modal analysis to find the natural frequencies of the system, and finally, a time-dependent analysis was performed to examine the dynamic response. A complete power harvesting analysis of a wave energy converter was modeled in COMSOL [19]. Fluid-structure interaction caused a power output in the PVDF device, which was simulated in 2D; the power extraction was modeled using an RC circuit: assuming the output voltage to be a sinusoid with the open-circuit voltage as its amplitude, the voltage across the load resistor and thus the power harvested could be calculated from the displacement and voltage signals. It did not take into account the slight damping due to the energy storage process, which would lower the steady-state response, but it showed that COMSOL is very capable of a quick, complete analysis.

## 1.4 Modeling of Membrane Vibrations

Of additional importance is a foundational knowledge of modeling the dynamics of pre-stressed membrane structures (see Figure 2). A paper by Jenkins and Tampi [20] documented experimental studies to validate theoretical relationships for membrane vibrations. The motivation was the modeling of local vibrations of a vibrating circular membrane for inflatable space structure applications. Noting that membrane structures have no inherent bending resistance, the governing equations for transverse vibration were derived by considering the membrane as a degenerate case of a plate. Solutions for the displacements and natural frequencies were given for varying boundary conditions and membrane geometries. The dynamic response was also calculated for a circular membrane due to harmonic excitation.

**Figure 1 The roof of the Denver International Airport, a prestressed membrane structure**

To capture the effect of prestress on membrane structures, Kukathasan and Pellegrino [21] studied the vibration of prestressed membranes for varying geometry (square, triangle, L-shape) using ABAQUS and compared their results with analytical solutions for the natural frequencies and mode shapes. It was found that the natural frequency does increase with prestress, due to the increase in stiffness.

## 1.5 Applications

As mentioned before, energy harvesting applications are myriad and growing, as ambient energy sources are omnipresent and the power requirements for potential applications continue to decrease. Anton and Sodano review several adaptations of piezoelectric energy harvesting technology; among them, wearable/implantable devices were presented, including a PZT dimorph-PVDF stave sole insert that harvests power from walking. The device produced 8.4 mW of power for a 500 kOhm resistance and a 0.9 Hz walking pace. The device was adapted for a US Navy work boot, and was found to consistently provide power to an RF identification tag [2]. Park et al. [22] detailed the power requirements and potential designs for an energy harvesting system aimed toward sensing and data acquisition for structural health monitoring networks. Browning et al. [23] documented the hardware design, ground and flight test results for an active control system for the F-16. The design utilized piezoelectric actuators in minimizing vibrations due to buffeting, which can cause structural failure.

## 1.6 Objectives and Approach

The objectives of this research were to create a computational model of a piezoelectric harvesting system using membrane vibrations, to devise a methodology for analyzing the harvesting capability of such a system, and to adapt the methodology for different cases. Attention was given to the computational speed of the methodology and the physical accuracy of the model. The computational model was generated using COMSOL 4.1. Tests were conducted to check the accuracy of the membrane model, and the piezoelectric coupling, the piezo-substrate interaction. A multi-step finite element analysis was formulated to include the prestress of the membrane, and a few sample cases were performed to demonstrate the capability of the model. The remainder of this thesis will describe in detail the work done to meet the goals of the research while fulfilling the criteria imposed above.

# Chapter 2

# Modeling Energy Harvesting From Membrane Vibrations In COMSOL

## Chapter 2.1 Problem Statement

The goal of this research was to develop a methodology to model energy harvesting from piezoelectric devices in a multiphysics code, COMSOL, with specific focus on membrane structures and their applications. Piezoelectric energy harvesting is becoming more popular due to an increased emphasis on renewable sources of energy, as well as the continued development of low-power wireless devices. One of the main issues that power harvesting addresses is the power supply of wireless devices built for autonomy (e.g. sensor networks for structural health monitoring, micro-air vehicles). Batteries have a limited lifetime and are difficult to maintain, as they require regular recharging and replacing. They thus constrain the range of the wireless device system unnecessarily. Energy harvesting is useful for increasing the portability, ease of maintenance and lifespan of these technologies. They can, in principle, perform continuous energy collection in unattended operation for an unlimited lifetime [2]. The prestressed membrane structures which these applications incorporate can generate large amplitude vibrations. This environment lends itself to vibrational energy harvesting via piezoelectric devices.

The transducers used for this study will be Smart Material's macro-fiber composites (MFCs), an example of which is shown in Figure 2. These specific materials were chosen for their increased

flexibility relative to generally brittle piezoceramics, while having a higher coupling coefficient than electroactive polymers like PVDF and ionic polymers. Electromagnetic and multi-modal harvesters have high power densities, but with their relative bulk, are too unwieldy for membrane structures. The cymbal transducer concept presented [6] is simply not tailored for the high-frequency/low-impact loading conditions examined here. Also, the interdigitated electrodes of the MFC allow for a '11' loading configuration, meaning the polarization is in the same direction as the induced stress/strain. This is suitable for membrane applications. An overview of the material data for the MFC, both in d31 and d33 loading conditions, is supplied in Table 1 [24].

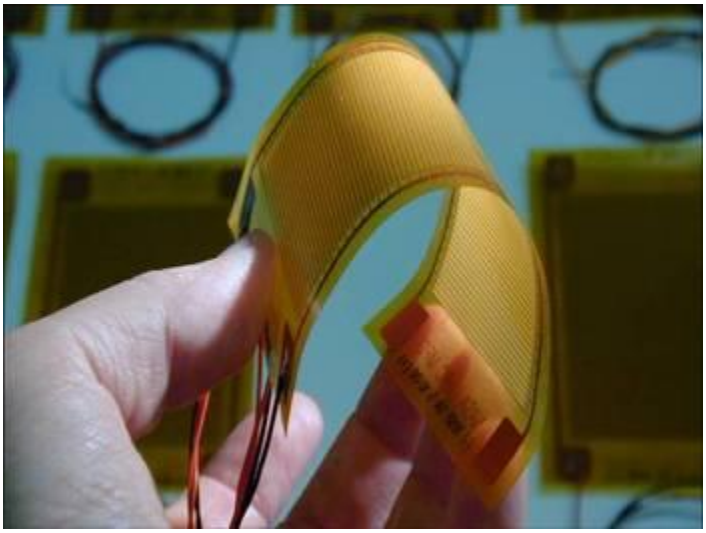

**Figure 2 A macro-fiber composite patch [24].**

Table 1 Material specifications for Smart Material Corp. Macro-Fiber Composite

| | |
|---|---|
| d31 | -2.1e-10 C/N for \|E\| > 1kV/mm; -1.7e-10 C/N for \|E\| < 1 kV/mm |
| d33 | 4.6e-10 C/N |
| Young's modulus | 30.336 GPa |
| Poisson's ratio | 0.31 |
| Typical thickness | 3e-4 m |
| Density | 5440 kg/m$^3$ |
| Operational voltage range | -500V to 1500V for d33, -60 V to 360V for d31 |

Though harvester devices based on a cantilevered beam/tip mass configuration have been modeled and thoroughly tested (for examples, refer to [10],[11],[12]), placing a piezo patch onto a flexible structure such as a prestressed, thin-film membrane is comparatively nascent. Those works which focused on membrane/plate-like structures either did not give an estimate for power harvesting capability [15], or did not examine prestressed membranes, which require a different model [16]. Prestressed membranes are ideal for this type of harvesting, as the natural frequencies can be tuned to the piezoelectric patches, while their flexibility allows for large amplitude vibrations. The interaction between the patches and the membrane substrate, as well as the effect of energy harvesting on the system, is not well understood. To circumvent the need for excess experimental testing, a simple and accurate means to assess the dynamic output of such a harvesting system is essential. Analytical methods are time-consuming and can become cumbersome to solve for increased complexity in the system, as closed-form solutions become more difficult to find. Efforts by Zurkinden et al. [18] and Emam [19] previously demonstrated that COMSOL is very capable of such a simple and complete analysis for energy harvesting application, but for less intensive problems. Using COMSOL is preferable to a coupled FEM-SPICE approach, as well. The coupling between the separate FEM and SPICE programs is explicit after each time step; the voltage and displacement data from FEM at $t_i$ would go into the PSPICE netlist, which would in turn calculate the voltage at $t_{i+1}$. That voltage data would feed back into the FEM via the constitutive relationships and so on. This makes the algorithm slow and expensive, while COMSOL 4.1 integrates both into one package, being created to handle multiphysics problems [17].

The following sections of this work will describe the successful efforts to engineer and implement a finite element model of piezoelectric energy harvesting from the ambient vibrations of a prestressed membrane structure. First, extensive model validation is presented, testing predictions of membrane natural frequencies, the interaction between the piezoelectric patch and the membrane, and

the electric coupling properties of the patch for harvesting applications. These results are compared to previous analytical studies with guidance from theory in order to gain confidence in the ability of the model to simulate piezoelectric energy harvesting systems. Then, the core analysis of this research will be discussed. Using techniques acquired from the literature search and model validation studies, the power harvested from the vibrations of a square prestressed membrane bonded with an MFC patch is calculated for a couple of different cases and compared with a determination of the dynamics from a separate study.

## 2.2 Model Validation

### 2.2.1 Membrane Vibrations

Membrane structures carry only tension and no compression/bending stress unless a preload is applied. In order to test that COMSOL 4.1 could accurately model the modal frequencies and response shapes of a prestressed membrane, as well as capture the effect of the prestress on the stiffness, a study was conducted comparing the 1st natural frequency of a prestressed square membrane to analytical calculations for varying prestress. The analytical calculations and model loading conditions come from Kukathasan and Pellegrino [21]. The problem describes a 0.2m x 0.2m square membrane made of Kapton ($\rho$ = 790 kg/m$^3$, $Y_1$=11.9 GPa, t = .1 mm, $\nu$ = .3). The Kapton membrane's four edges are constrained in the 3-direction (vertical displacement), while a prestress is induced in the 1 and 2 directions (in-plane). Kukathasan and Pellegrino solved for the natural frequencies in terms of geometric dimensions, material properties and loading conditions from the governing equation of transverse motion. The analytical equation used to produce the comparisons is reproduced below. The subscripts $m$ and $n$ designate the mode, $a$ and $b$ are side lengths, T is the prestress and M is the mass per unit area.

$$\omega_{mn} = \pi c \sqrt{\frac{m^2}{a^2} + \frac{n^2}{b^2}}, c = \sqrt{\frac{T}{M}} \tag{20}$$

The COMSOL 4.1 procedure starts by choosing the Solid Mechanics physics of the Structural Mechanics module, and setting up an eigenfrequency analysis. The geometry is added by defining the membrane as a thin 3D block; the material data is added afterward. To incorporate the prestress, COMSOL 4.1 has the option to include geometric nonlinearities in the analysis. Then, prescribe the prestress (given by [21] as force/length, but added here as force/area) in the Initial Stress and Strain subnode. Fix the boundaries on the four sides with a prescribed displacement of w = 0, and mesh by sweeping quadrilaterals through the assembly. The eigenfrequency analysis takes the initial conditions of the prestress into account in the calculation of the natural frequencies. Figure 3 displays the first four mode shapes from the resulting study, not counting the duplicates of the coupled modes.

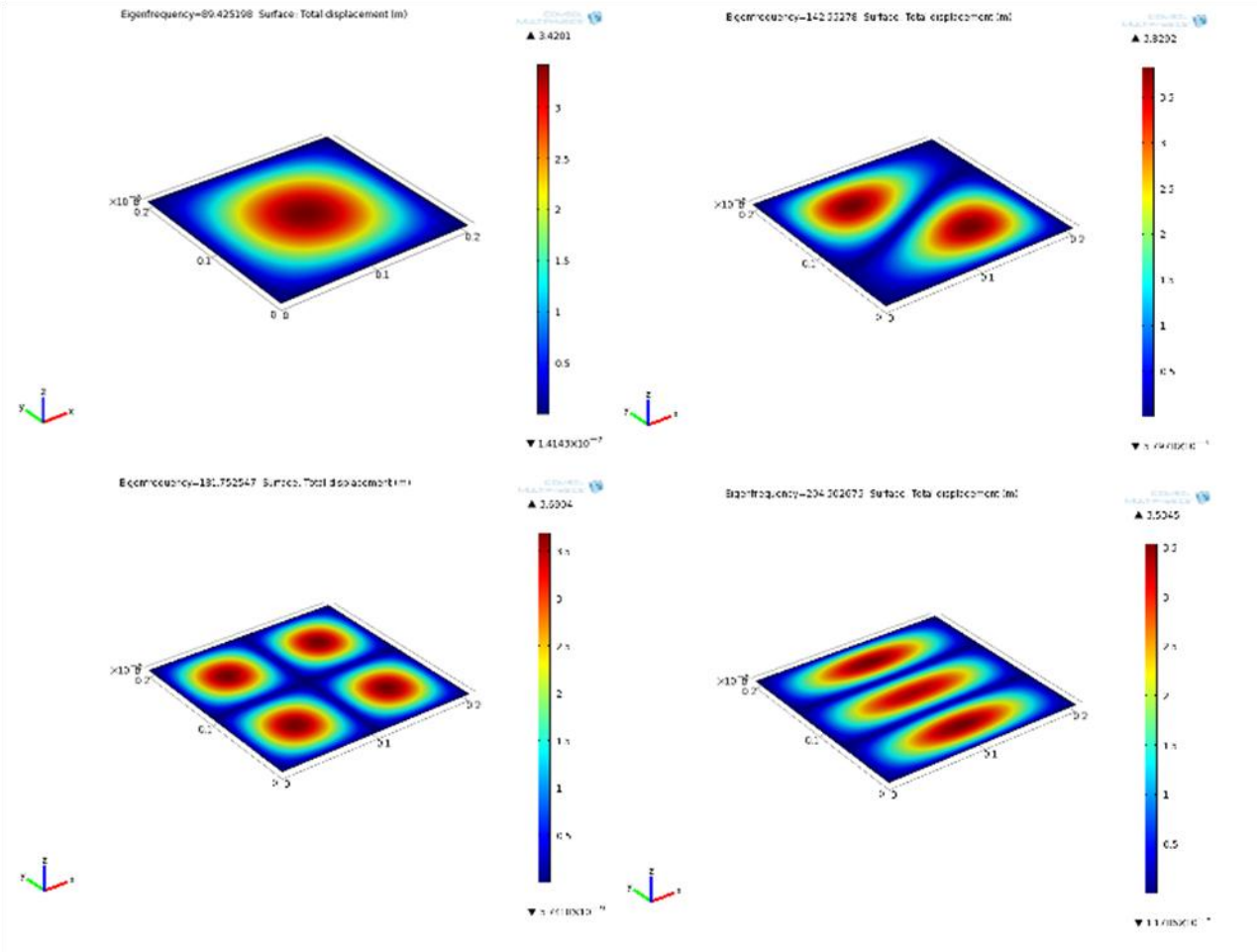

**Figure 3 First four mode shapes for membrane validation.**

Table 2 shows the results of the comparison between analytical calculations and the FE method from

COMSOL 4.1. For varying prestress, COMSOL 4.1 accurately captures the added stiffness, which causes the increase in the first natural frequency.

Table 2 First natural frequency vs. prestress, comparing analytical with COMSOL

| Prestress (N/m) | Analytical Freq. (Hz) | COMSOL freq. (Hz) |
|---|---|---|
| 10 | 39.78 | 40.84 |
| 20 | 56.25 | 57.01 |
| 30 | 68.9 | 69.51 |
| 40 | 79.56 | 80.09 |
| 50 | 88.95 | 89.43 |

A fine mesh of 356 elements were used to produce these results, after the mesh was shown to converge around that density. Figure 4 shows the convergence plot of natural frequency versus the log of the number of elements.

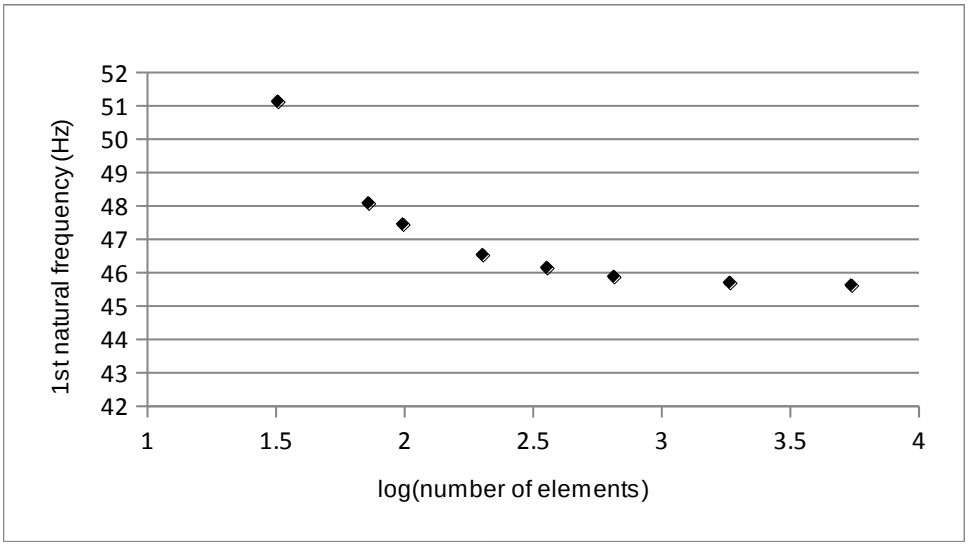


**Figure 4 Mesh convergence plot for membrane validation test**

2.2.2. Piezo-Substrate Interaction

The complexity of the structural dynamics is increased when adding a piezoelectric patch onto the membrane substrate. In the bonding process, the patch is not preloaded along with the membrane, and this can be difficult to model. To verify that the model can reproduce this process as well as agree

with theoretical predictions, a nylon square membrane is coupled with a piezoelectric patch on its surface. Variance in the first natural frequency was studied for changes in several parameters. As before, a prestress is loaded biaxially on the membrane (but, again, not the patch); however, now the membrane is fixed with an encastre condition on its four sides.

The modeling procedure is slightly different this time. Selecting the Piezoelectric Devices physics from the Structural Mechanics module with an eigenfrequency analysis, the membrane geometry is set up the same way as before, changing the dimensions to 0.5m x 0.5m x 0.001m. The 0.1m x 0.1m x 0.001m patch is then added as a thin 3D block on top of the membrane depending on the location. The material data is added afterward, followed by the application of the prestress (10 N/m). To avoid loading the piezoelectric material, only the membrane subdomain is selected. The fixed boundary conditions are applied next, as well as the electrical boundary conditions for the system. The bottom of the piezo patch (where it meets the substrate) is grounded, while the top is left as a floating potential; the membrane is not electroactive. The first natural frequencies as well as the mode shapes and normalized maximum displacements associated with them were determined for varying patch thickness and location, as well as turning the piezoelectric coupling on and off. Figure 5 depicts the trend of the 1st natural frequency's change for varying patch thickness, where the patch is located at the corner of the membrane. Figure 6 shows the model output for a patch thickness of 5 mm; note the slight lack of radial symmetry for the mode shape around the piezoelectric patch. Increasing the thickness of the piezoelectric patch increases the natural frequency of the system, implying that an increase in thickness means added stiffness for less change in the mass of the system. Considering the relative small size of the patch compared with the substrate in addition to the piezo's greater stiffness, the results correlate well with theoretical expectations.

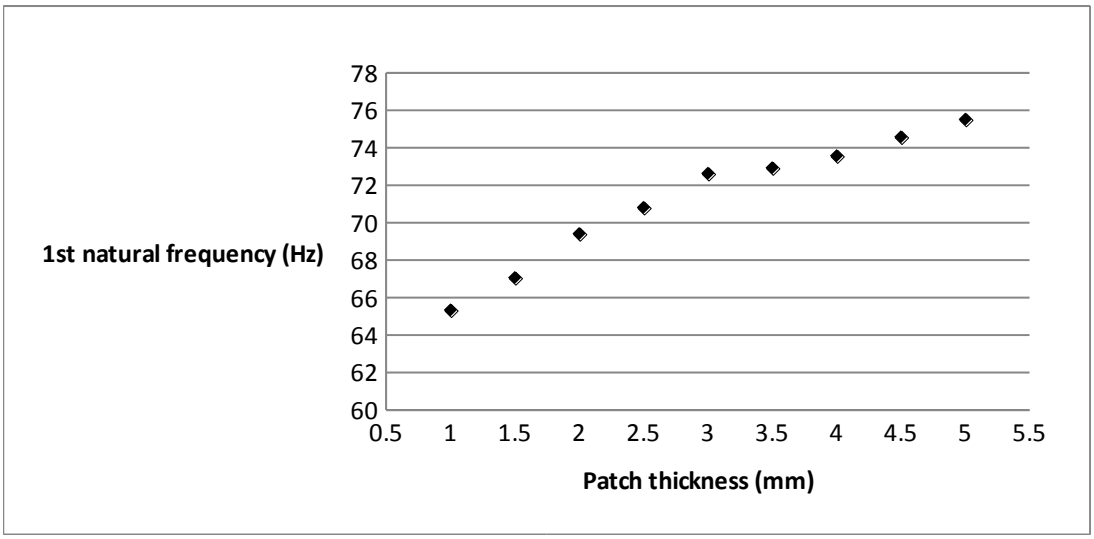


**Figure 5 First natural frequency vs. patch thickness for square membrane study**

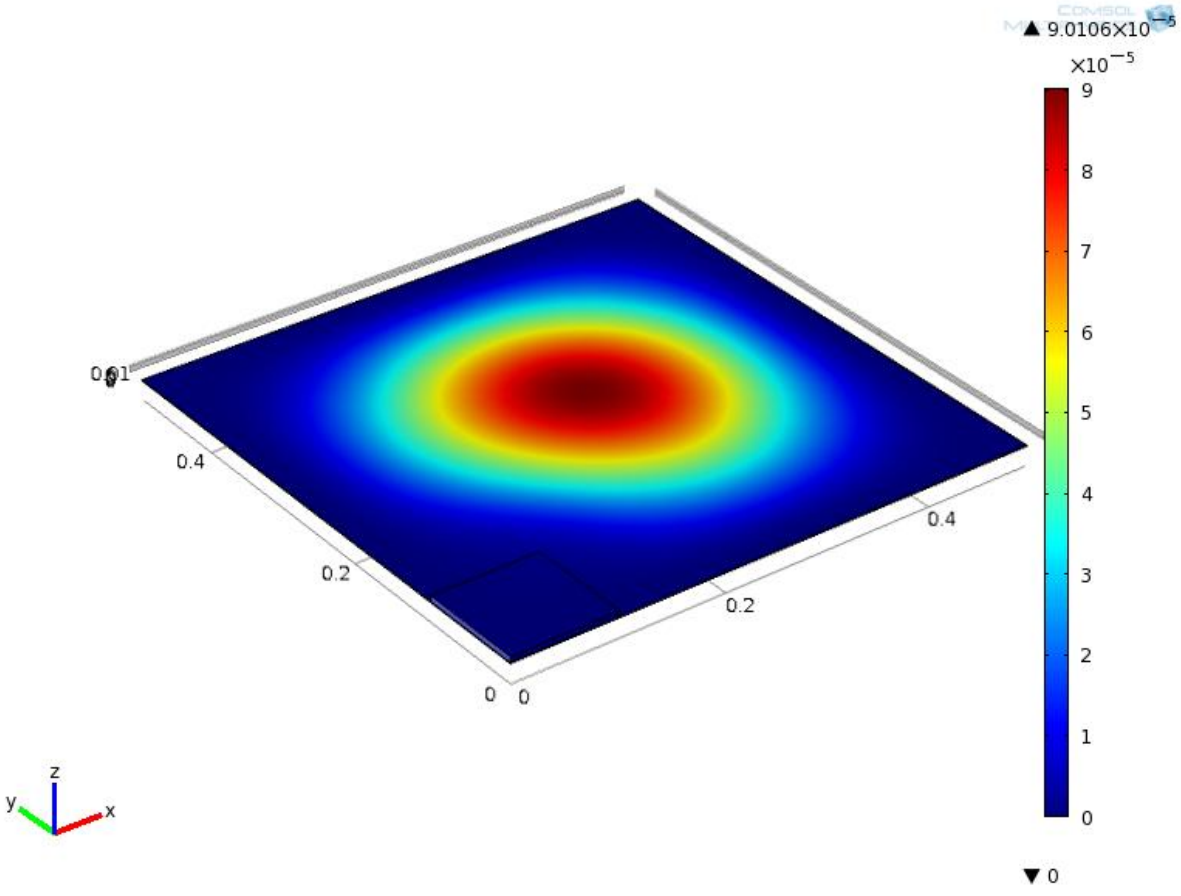


**Figure 6 First mode shape for square membrane study, patch thickness = 5 mm**

Table 3 shows the results of varying patch location (thickness of 1 mm) between the corner, the side median (center of patch is at $(x, y)$ = (.25, .05) [m]), and the center of the membrane.

Table 3 1st natural frequency and max. normalized displacement vs. patch location

| Patch location | 1st natural frequency (Hz) | Max. normalized displacement (m) |
|---|---|---|
| Corner | 65.342 | 1.26E-04 |
| Side median | 71.986 | 1.28E-04 |
| Center | 51.185 | 5.27E-05 |

Placing piezoelectric patches on areas of higher strain (near the fixed boundaries) increases the stiffness of the system and thus the natural frequencies. Placing them on areas of higher deformation decreases the response but also the stiffness. Figures 7 and 8 show the results of the center and side median solutions, respectively.

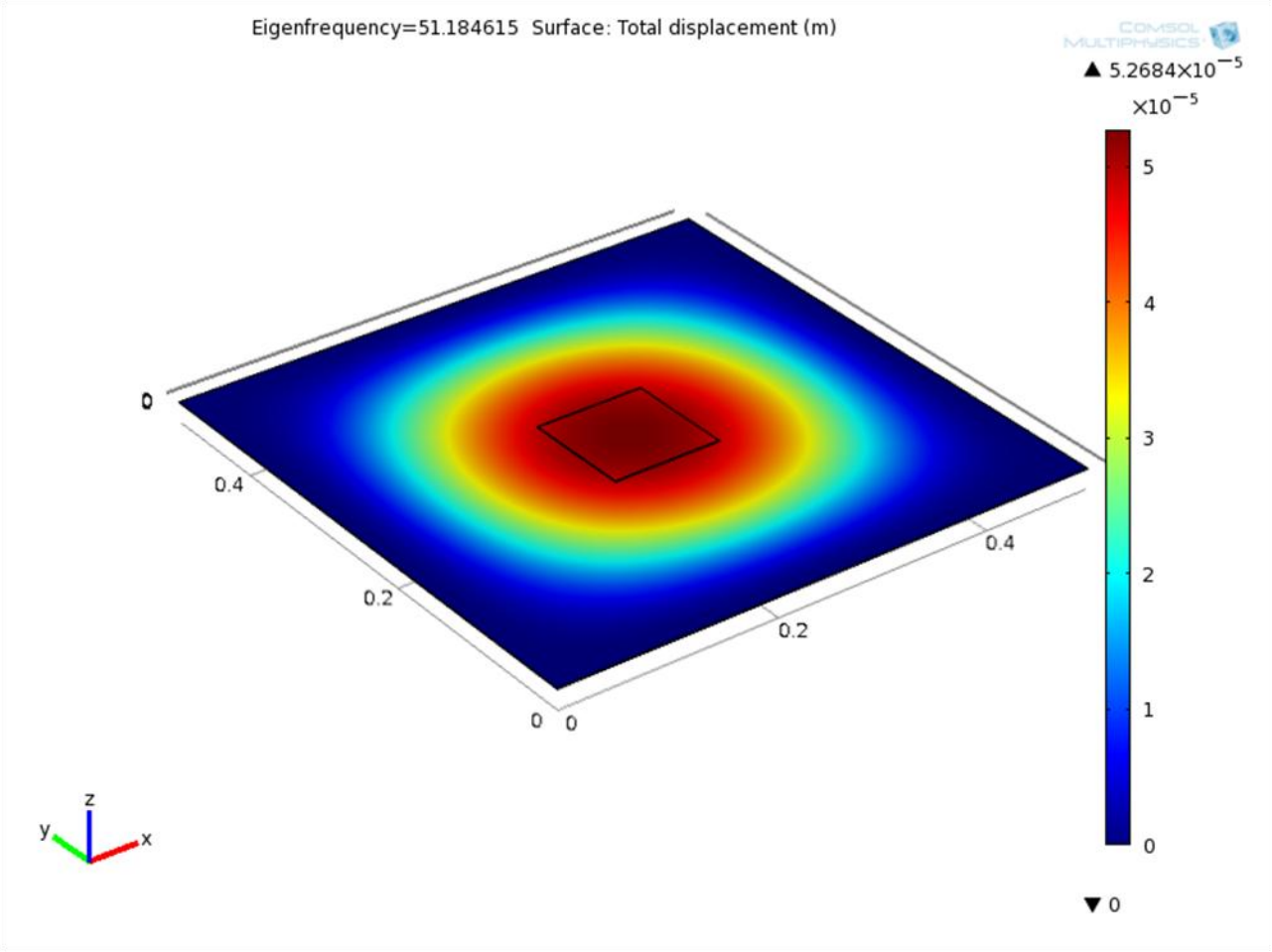


**Figure 7 First mode shape for square membrane study, patch located at center**

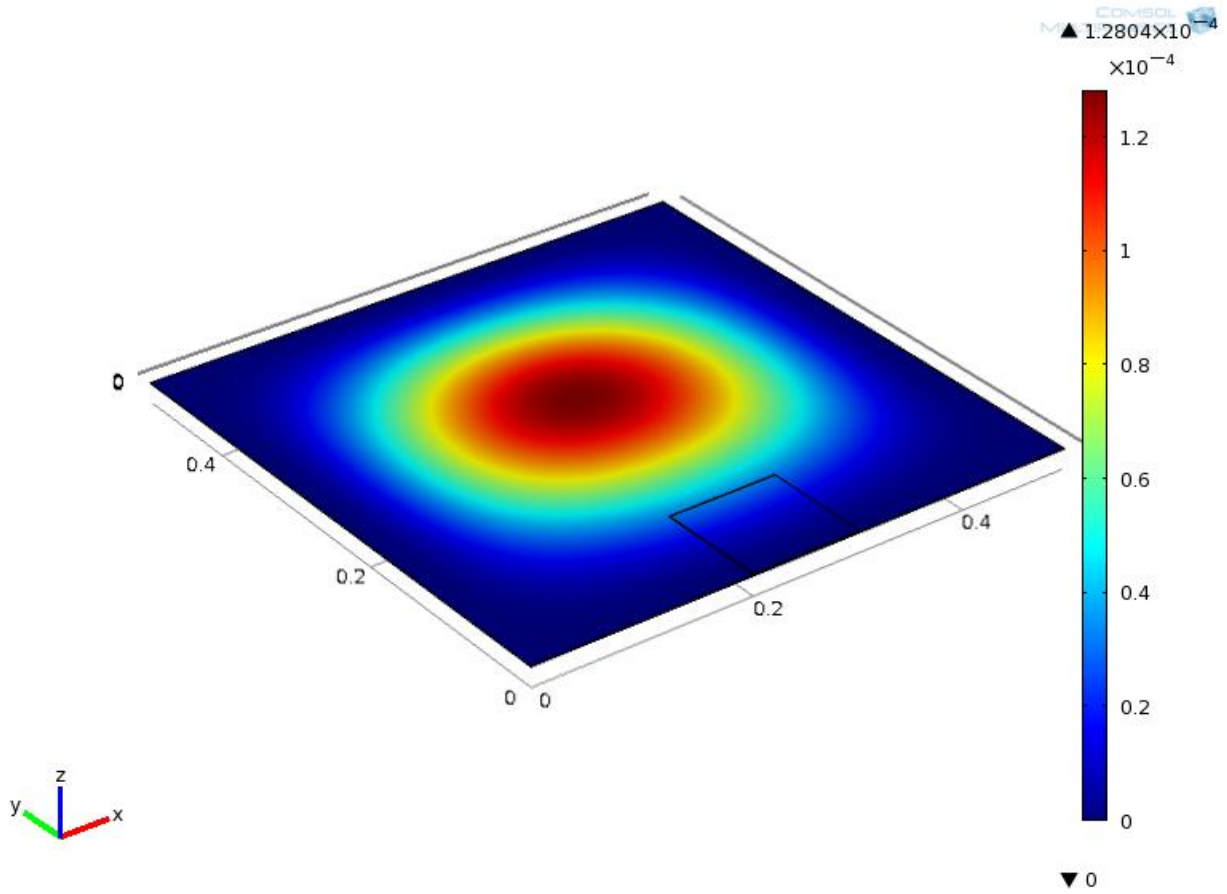


**Figure 8 First mode shape for square membrane study, patch located at side median**

Laying the foundation for a full-fledged harvesting analysis, the electrostatic side of the piezo model was tested. For a simple case of a 31-extender as found in [1], the transducer equations relating applied force and voltage to displacement and charge density can be found with a certain amount of ease. The 1m x 1m unimorph piezo material is fixed on one end and axially loaded on the other. After setting up the physics, geometry and material data, the boundary conditions are applied; the bottom of the extender is the ground, while the top is loaded with an electric potential of 1V. The free face of the material is either loaded axially with 100N (applied as a pressure) or, in the case of the static capacitance test, is unloaded. Figures 9 and 10 display the results of the axial stiffness and static capacitance tests for this textbook problem. Since the piezoelectric capacitance $C_p$ = Q/V and the surface charge comes from integrating over the electroded area, the capacitance was found to be 9.595e-7 Farads, as compared to an analytical estimate of 8.854e-7 Farads (less than 10% difference).

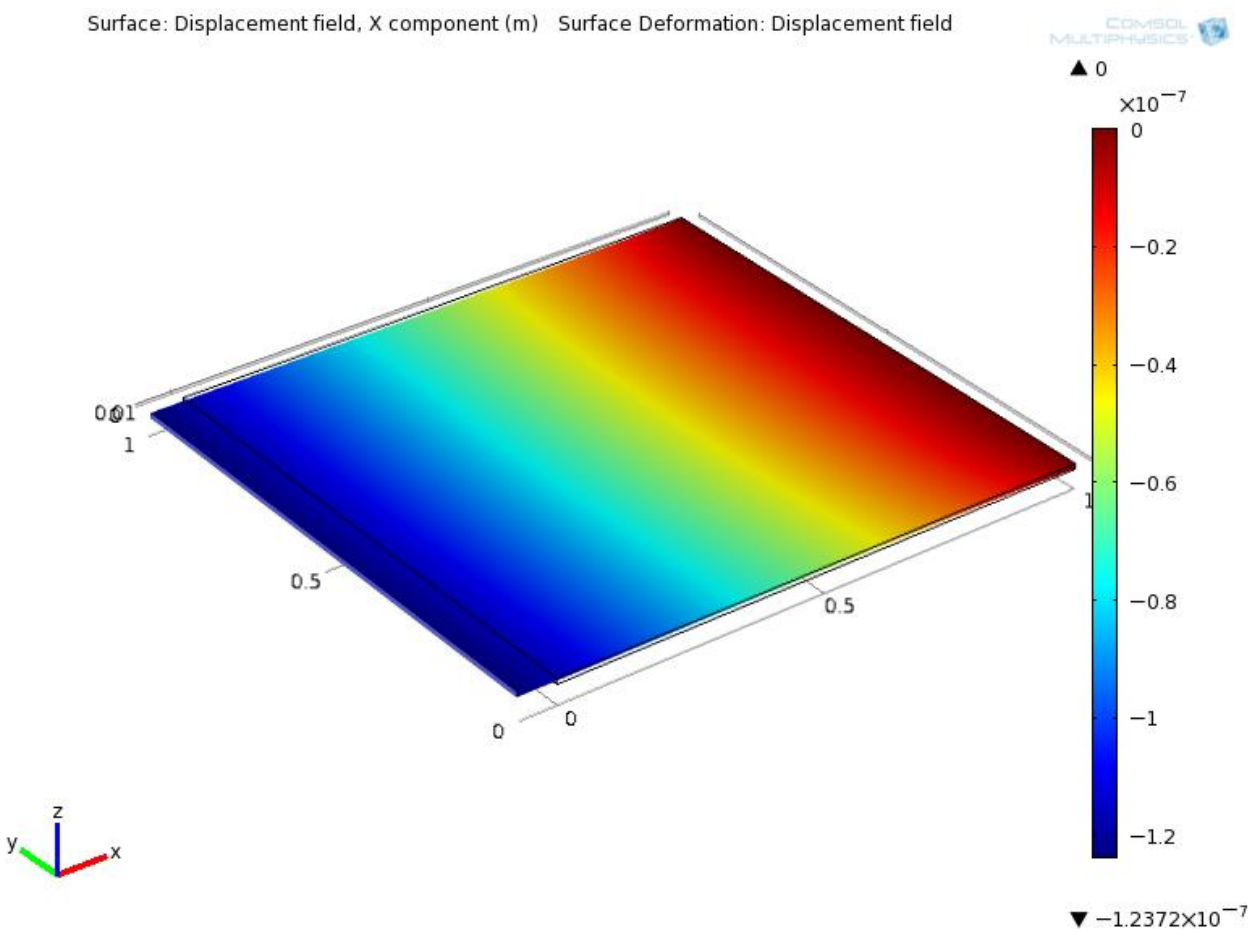


**Figure 9 Displacement in 31-mode extender, axial stiffness test**

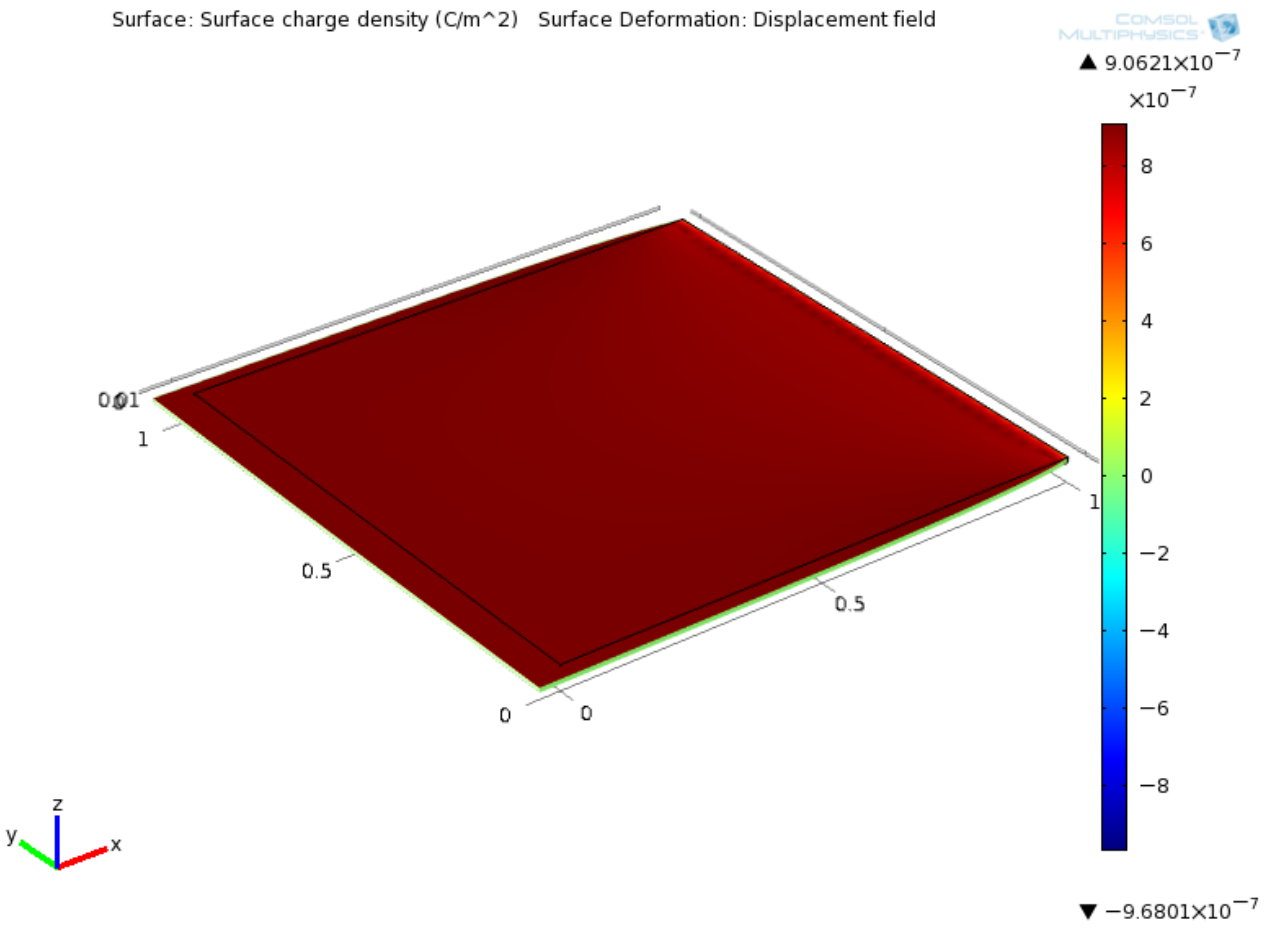


**Figure 10 Surface charge density for 31-mode extender, static capacitance test**

## 2.3 Membrane Vibration Harvesting Analysis

Demonstrating the contribution to knowledge, a complete power analysis of a piezoelectric energy harvesting system for two different loading cases is presented in detail. The system in question is a single piezoelectric patch placed onto a prestressed square nylon membrane which is fixed-fixed in both in-plane directions. The bottom of the membrane is excited with a harmonic pressure load in the out-of-plane direction, causing a sinusoidal deformation in the patch, and thus a voltage output. The harvesting is taken into account via a load resistor.

### 2.3.1 Model Set-up

As this system involves the conversion of mechanical strain energy into electrical power, the

piezoelectric patch can be modeled as a generator, while the harvesting process was modeled as a dissipater. From a circuit system standpoint, the sinusoidal form of the loading meant that the piezoelectric patch could be modeled as an AC voltage source in series with a capacitor, which represents the dielectric properties of the material. An equivalent circuit for the described problem is shown in Figure 11.

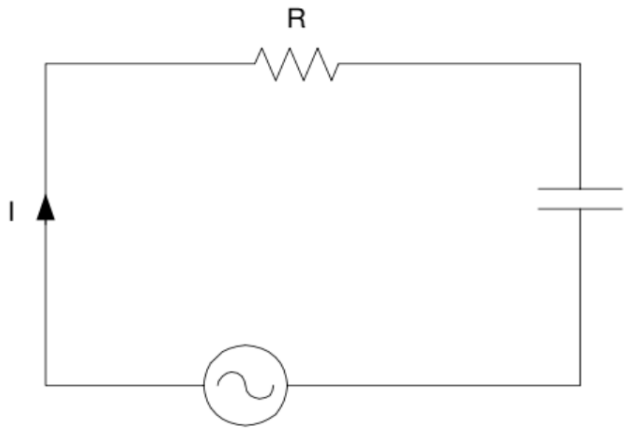


**Figure 11 Equivalent circuit diagram for the harvester**

After conducting a modal analysis to determine the natural frequency of the system, a time-dependent analysis is conducted to simulate the dynamic response of the harvester to the harmonic excitation. Displacement and voltage data can be collected, while a variant of Ohm's law is used to calculate the power harvested in conjunction with the application of the load resistor.

2.3.2 Procedure

As before, the Piezoelectric Devices physics from the Structural Mechanics module is chosen for the model. First, an eigenfrequency analysis must be performed to determine the natural frequency and thus the excitation frequency of the system. After setting up the geometry and boundary conditions, the assembly was meshed and analyzed.

Next, disabling the eigenfrequency analysis, the excitation load was applied. Defining the appropriate parameters w and $F_0$ (40 $N/m^2$), a time-dependent analysis was run to determine the

harvesting capabilities of the system. Displacement and voltage data were collected from the ungrounded top face of the piezoelectric patch and plotted against time. Results for two specific cases are presented below.

### 2.3.3 Results

For a 0.5 x 0.5 x 0.001 m nylon membrane with a 0.1 x 0.1 x 0.001 m patch at its corner, the first natural frequency is ~65 Hz, so the excitation frequency was set to 50 Hz. The patch's size is a little wider than the largest of available $d_{33}$ effect patches, but a square geometry was chosen for the purposes of simply demonstrating the model's capability. A Rayleigh damping coefficient of $b$ = 0.1 was used to incorporate structural damping into the system. After reaching steady state, displacement, voltage and power vs. time for a resistance of 100 Ohms are shown in Figures 12-14. Also, the voltage output on the extraction surface is shown in Figure 15. The maximum power output for this configuration is ~10 microwatts.

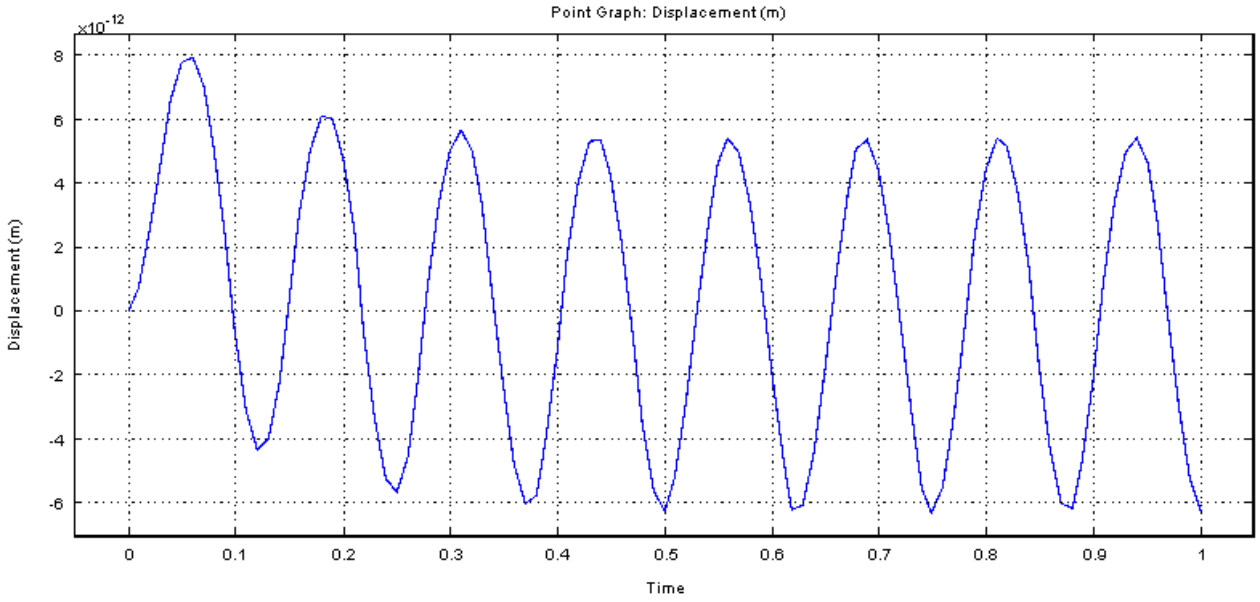


**Figure 12 Displacement vs. time for patch data extraction point, corner case**

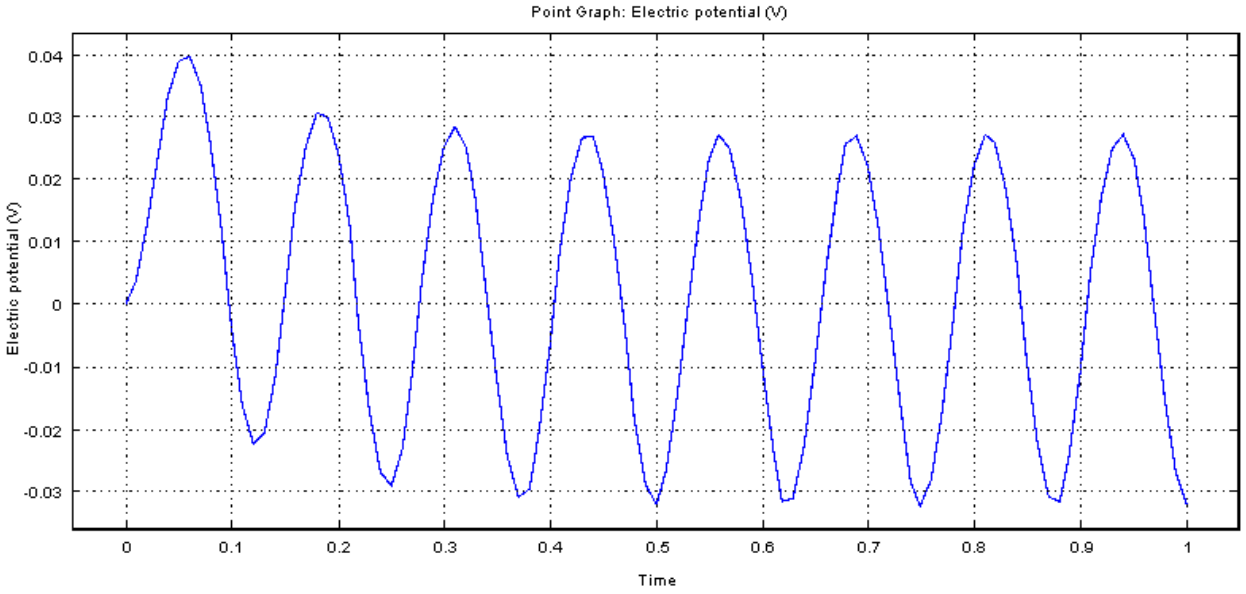


**Figure 13 Voltage vs. time for patch data extraction point, corner case**

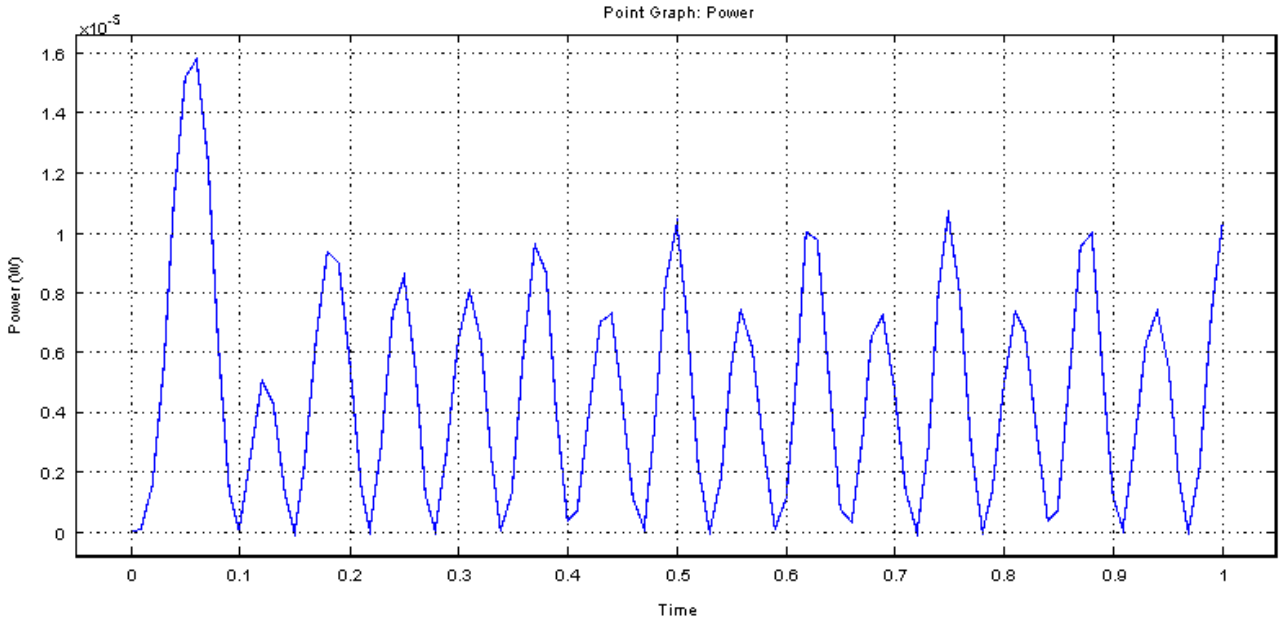


**Figure 14 Power harvested vs. time for patch data extraction point, corner case**

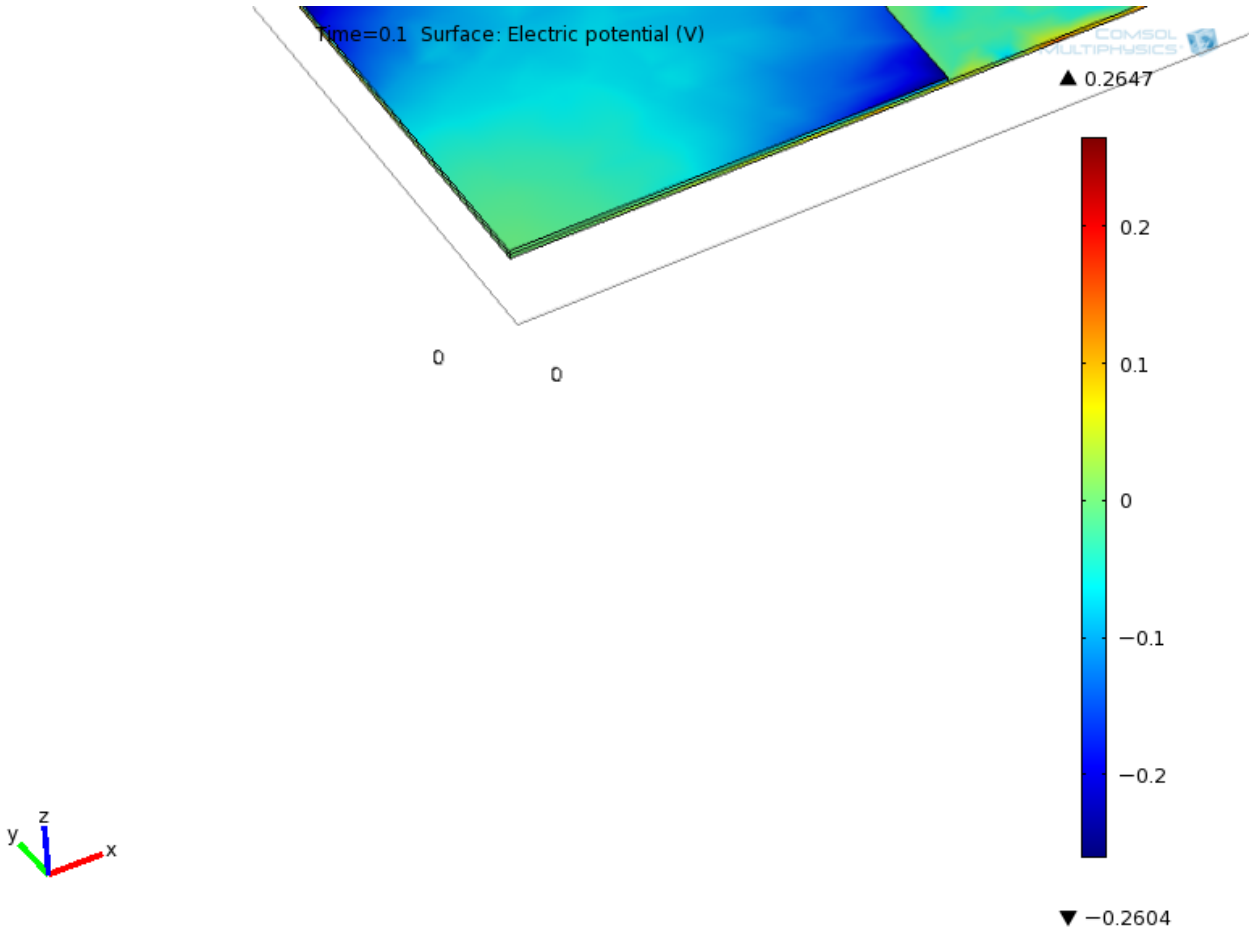


**Figure 15 Voltage surface plot at t = 1s, corner case**

For a case where the patch is at the side median, the excitation frequency was placed closer to resonance. Using the same resistance, displacement, voltage and power vs. time plots were generated as in Figures 16-18. The voltage output on the extraction surface is again shown in Figure 19. The maximum power output for this configuration is much greater due to the voltage increase, on the order of ~ 0.1 W. The increase in response for the voltage is a direct result of the near-resonant loading condition (note that the displacement increase is three orders of magnitude larger because of this).

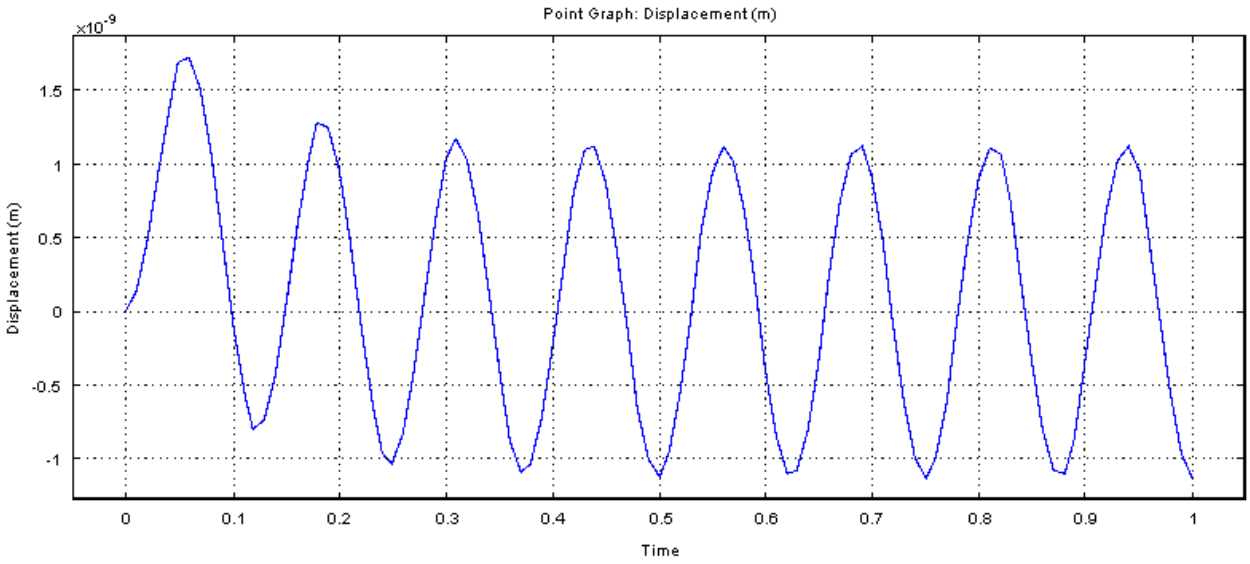


**Figure 16 Displacement vs. time for patch data extraction point, side case**

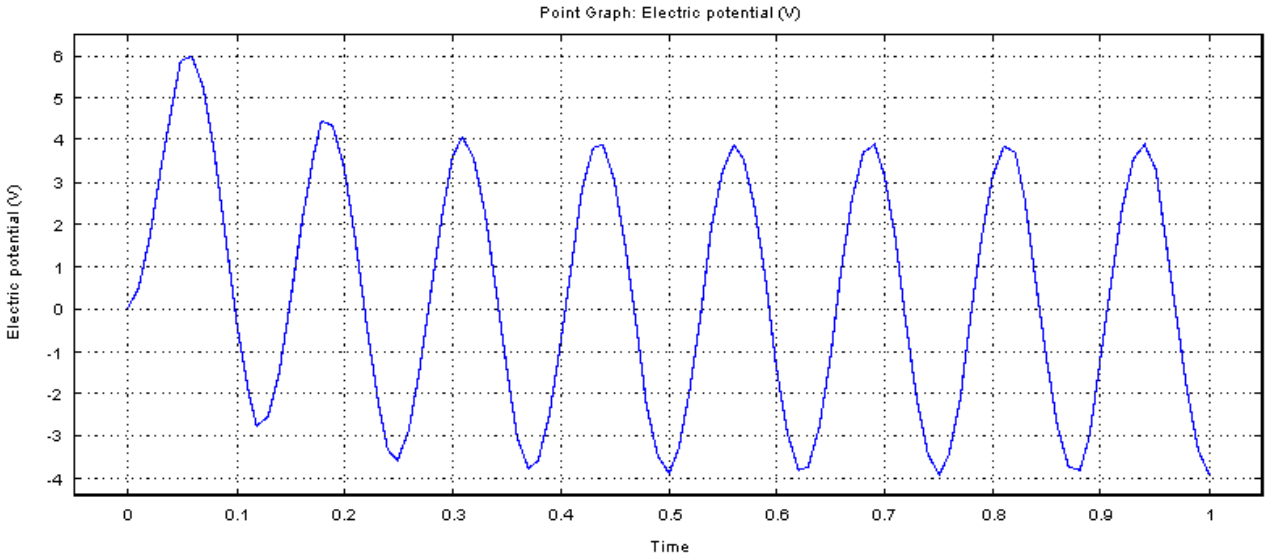


**Figure 17 Voltage vs. time for patch data extraction point, side case**

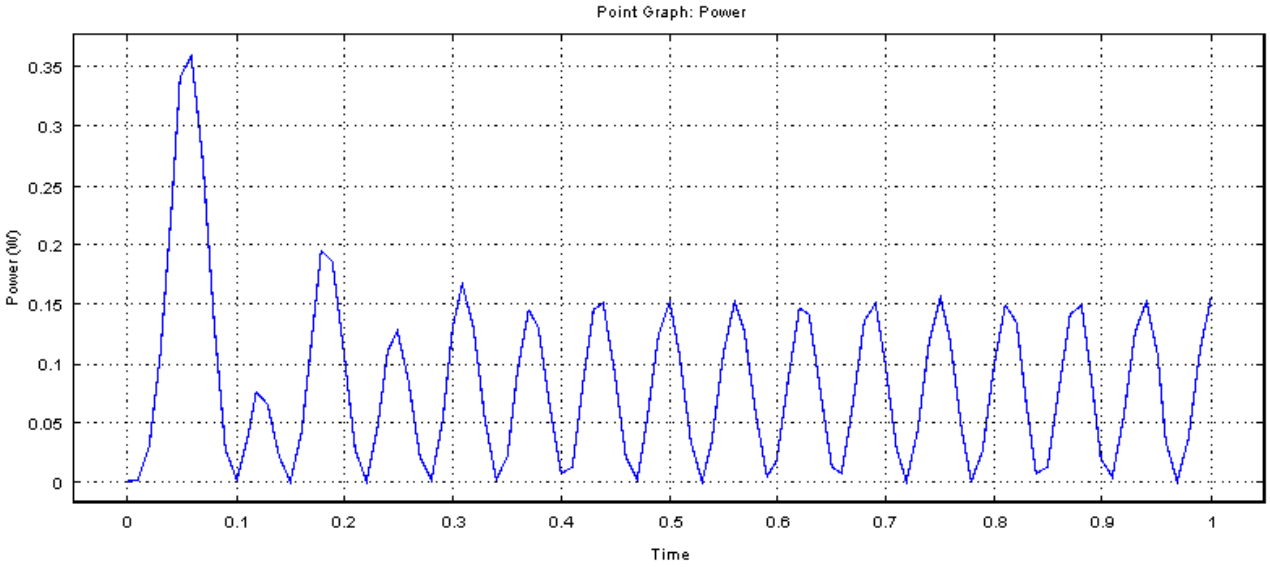


**Figure 18 Power harvested vs. time for patch data extraction point, side case**

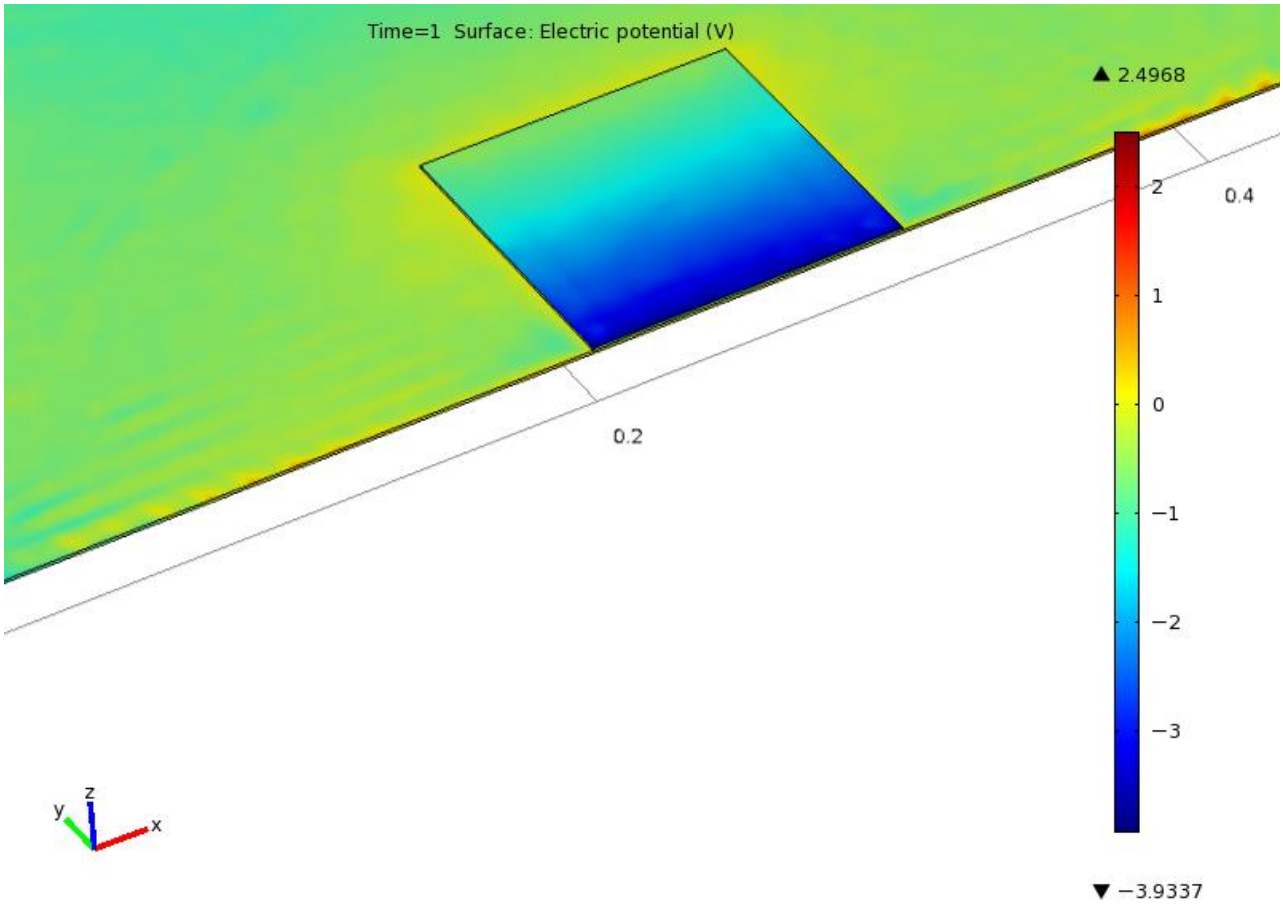


**Figure 19 Voltage surface plot at t = 1s, side case**

Placing the patch at the center of the membrane, the excitation frequency was lowered to prevent divergence in the solution due to resonance. For the same resistance, the displacement, voltage and power harvested were tracked over a time of 1 second. The results are shown in Figures 20-22. The maximum power output was on the order of ~.1 W, equivalent to the response from placing the patch at the side of the membrane.

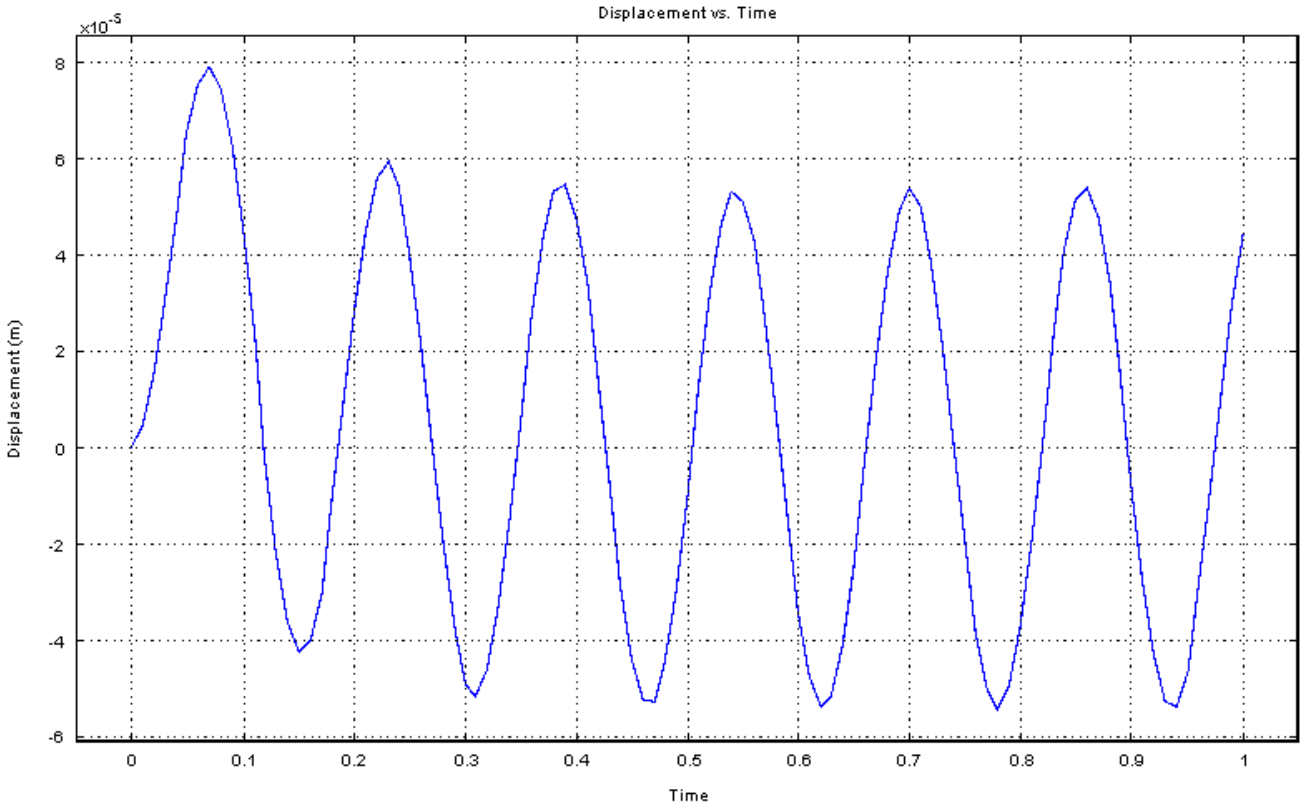


**Figure 20 Displacement vs. time for patch data extraction point, center case**

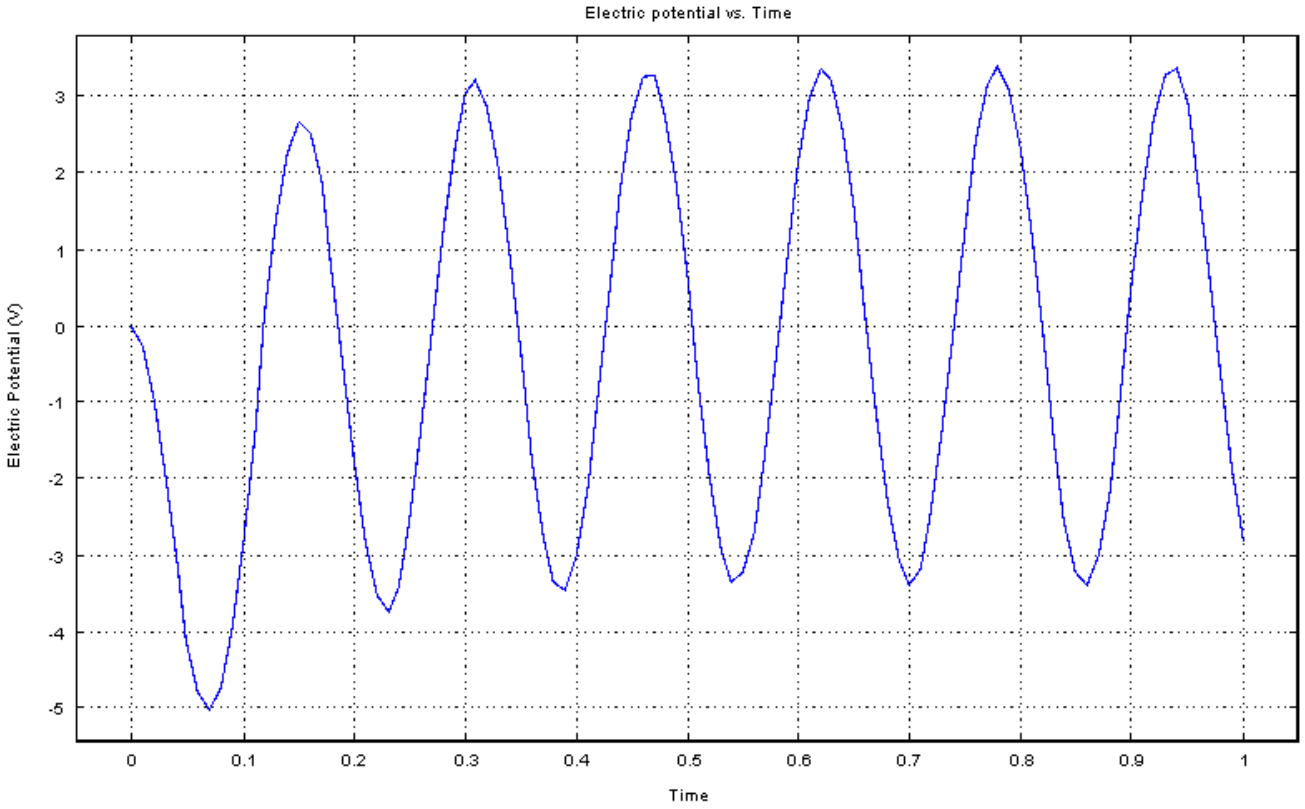


**Figure 21 Voltage vs. time for patch data extraction point, center case**

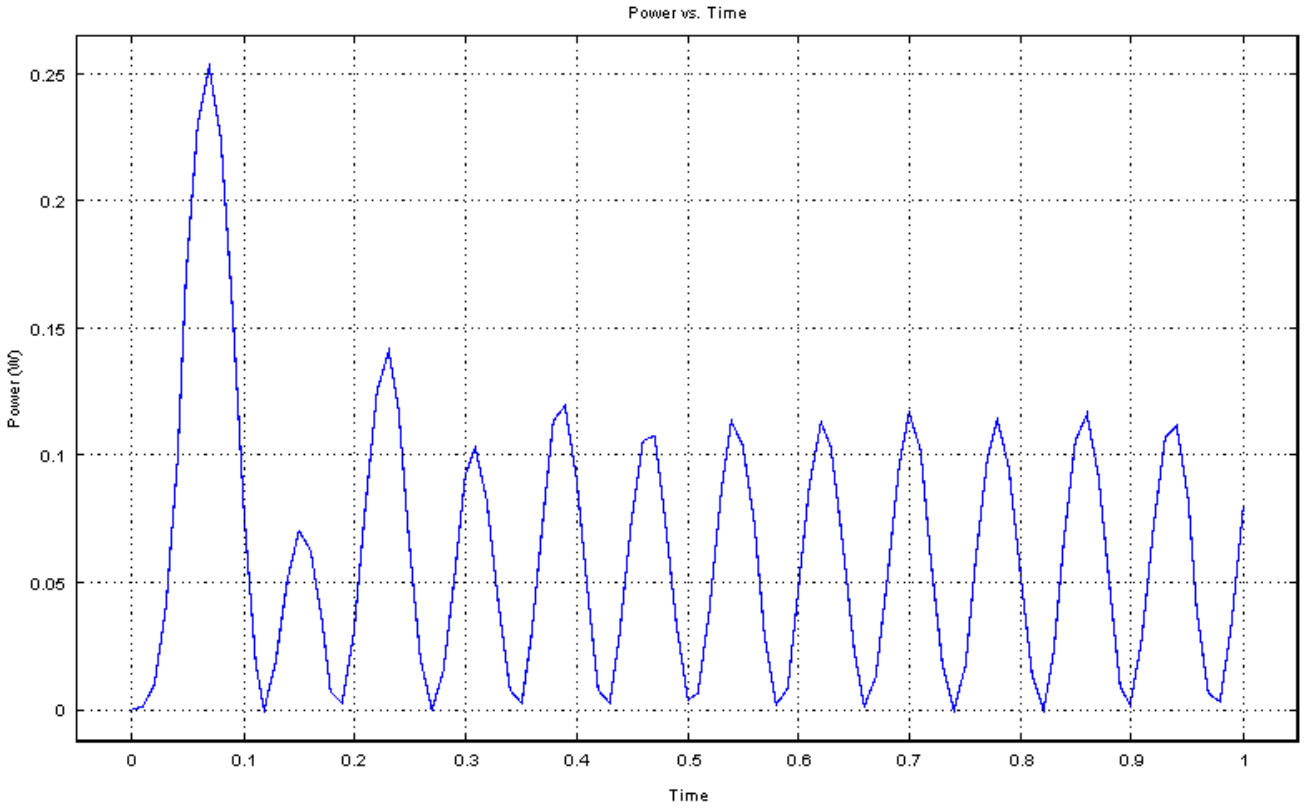


**Figure 22 Power harvested vs. time for patch data extraction point, center case**

A parametric study was also conducted, varying the load resistance to confirm the relationship between the power harvesting system and the resistive load it is connected to. The resulting plot for a parameter sweep between 10 and 5000 Ohms is seen in Figure 23. For a greater resistance, the equivalent circuit dampens the vibration response of the membrane, allowing for smaller amplitudes.

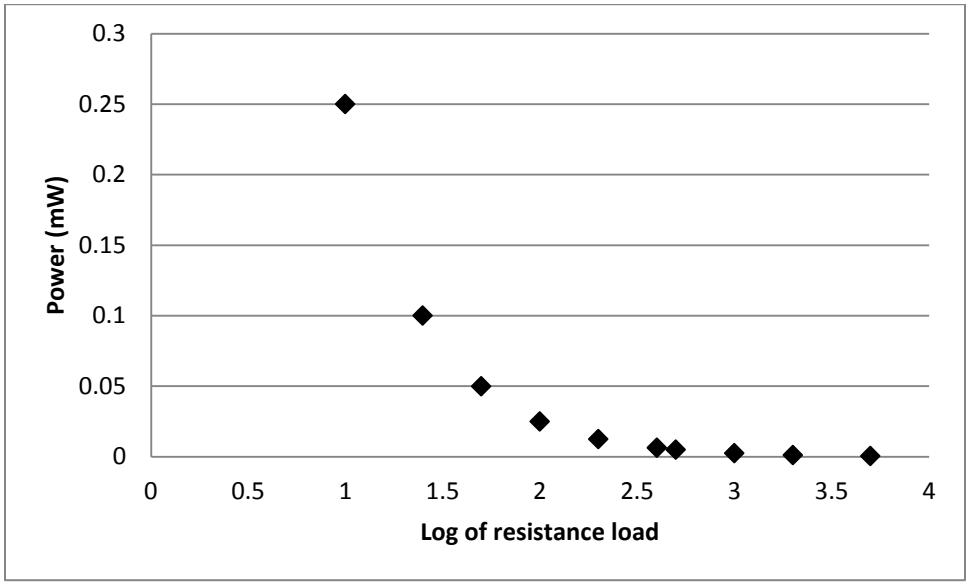


**Figure 23 Max. power vs. logarithm of load resistance, corner case**

Thus, it has been demonstrated that the developed algorithm for modeling the membrane energy harvester in COMSOL 4.1 can produce meaningful, accurate results with relative simplicity and ease.

# Chapter 3

# Summary

The results of the test cases show that the model developed can predict the energy harvesting process from the vibrations of prestressed membranes. The maximum power output was on the order of microwatts to milliwatts, which was verifiable with respect to previous work. The algorithm is flexible enough such that parametric studies can be conducted to determine such relations as power harvested versus load resistance. In addition to this, the methodology is adaptable for any membrane shape, material, prestress, and thickness, as well as patch material, thickness and location.

Future work could entail the exploration of these cases, and their applications to design and optimization. For instance, for a given number of patches, this method could be used to determine what locations would yield the best harvesting capabilities, perhaps using a genetic algorithm. Experimental work is also suggested to further verify the computational solutions. Collecting various types of flexible piezoceramics and arranging them upon a prestressed membrane structure, one could excite the membrane with accelerometers and test the induced voltages.

Chapter 4

# Bibliography

1.) Leo, D.J., *Engineering Analysis of Smart Material Systems*, Wiley, Hoboken, NJ, 2007.

2) Anton, S.R. and Sodano, H.A., "A Review of Power Harvesting Using Piezoelectric Materials (2003-2006)", *Smart Materials and Structures*, Vol. 16, 2007, pp.1-21.

3) Martin, B.R., "Energy Harvesting Applications of Ionic Polymers", Master's Thesis, Department of Mechanical Engineering, Virginia Polytechnic and State University, Blacksburg, VA, 2005.

4) Sodano, H.A., Lloyd, J., and Inman, D.J., "An Experimental Comparison Between Several Active Composite Actuators for Power Generation", *Proceedings of SPIE,* Vol. 5390, Bellingham, WA, 2004, pp. 370-378.

5) Yang, Y., Tang, L., and Li, H., "Vibration Energy Harvesting Using Macro-fiber Composites", *Smart Materials and Structures*, Vol. 18, 2009.

6) Kim, H.W., Priya, S., Uchino, K., and Newham, R.E., "Piezoelectric Energy Harvesting Under High Pre-stressed Cyclic Vibrations", *Journal of Electroceramics*, Vol. 15, 2005, pp. 27-34.

7) Minazara, E., Vasic, D., Costa, F., and Poulin, G., "Piezoelectric Diaphragm for Vibration Energy

Harvesting", *Ultrasonics*, Vol. 44, 2006, pp. 699-703.

8) Beeby, S.P. et al., "A Micro-electromagnetic Generator for Vibration Energy Harvesting", *Journal of Micromechanics and Microengineering*, Vol. 17, 2007, pp. 1257-1265.

9) Dong, S., Zhai, J., Li, J.F., Viehland, D., and Priya, S., "Multimodal System for Harvesting Magnetic and Mechanical Energy", *Applied Physics Letters*, Vol. 93, 2008, pp. 103511-1-103511-3.

10) Sodano, H.A., Park, G., and Inman, D.J., "Estimation of Electric Charge Output for Piezoelectric Energy Harvesting", *Strain*, Vol.40, 2004, pp. 49-58.

11) Erturk, A. and Inman, D.J., "A Distribute Parameter Electromechanical Model for Cantilevered Piezoelectric Energy Harvesters", *Journal of Vibration and Acoustics*, Vol. 130, Aug. 2008.

12) Khameneifar, F., Moallem, and M., Arzanpour, S., "Modeling and Analysis of a Piezoelectric Energy Scavenger for Rotary Motion Applications", *Journal of Vibration and Acoustics*, Vol. 133, Feb. 2011.

13) Hagood, N.W. and Von Flotow, A., "Damping Of Structural Vibrations With Piezoelectric Materials and Passive Electrical Networks", *Journal of Sound and Vibration*, Vol. 146, 1991, pp. 243-268.

14) Corr, L.R. and Clark, W. W., "Energy Dissipation Analysis of Piezoceramic Semi-Active Vibration Control", *Journal of Intelligent Material Systems and Structures*, Vol. 12, Nov. 2001, pp. 729- 736.

15) Taleghani, B., "Validation of High Displacement Piezoelectric Actuator Finite Element Models", ARL TR-2253, Aug. 2000.

16) Kim, S., Clark, W. W., Wang, Q., "Piezoelectric Energy Harvesting with a Clamped Circular Plate", *Journal of Intelligent Material Systems and Structures*, Vol. 16, Oct. 2005, pp. 847-854.

17) Elvin, N.G. and Elvin, A.A., "A Coupled Finite Element - Circuit Simulation Model for Analyzing Piezoelectric Energy Generators", *Journal of Intelligent Material Systems and Structures*, Vol. 20, Mar. 2009, pp. 587-595.

18) Emam, M., "Finite Element Analysis of Composite Piezoelectric Beam Using COMSOL", Master's

Thesis, Drexel University, Philadelphia, PA, 2008.

19) Zurkinden, A.S., Campanile, F., and Martinelli, L., "Wave Energy Converter through Piezoelectric Polymers", *Proceedings of the COMSOL Users Conference*, Grenoble, France, 2007.

20) Jenkins, C.H. and Tampi, M., "Local Membrane Vibrations and Inflatable Space Structures", *SPACE 2000*, AIAA, Long Beach, CA, 2000, pp. 410-416.

21) Kukathasan, S. and Pellegrino, S., "Vibration of Prestressed Membrane Reflectors", European Space Agency, ESA-TR194, Mar. 2001.

22) Park, G., Rosing, T., Todd, M. D., Farrar, C. R., and Hodgkiss, W., "Energy Harvesting for Structural Health Monitoring Sensor Networks", Los Alamos National Laboratory, LA-14314-MS, Feb. 2007.

23) Browning, J.S., Cobb, R.G., Canfield, R.A., and Miller, S.K., "F-16 Ventral Fin Buffet Alleviation Using Piezoelectric Actuators", *50$^{th}$ AIAA Structures, Structural Dynamics, and Materials Conference*, Palm Springs, California, 2009.

24) "MFC", Smart Material Corp., Sarasota, Florida, November 2011. [http://www.smart-material.com/MFC-product-main.html Accessed 12/9/11.]

25) "Predefined Multiphysics Interfaces," *COMSOL Structural Mechanics Module User's Guide*, COMSOL AB, USA, 2010, pp. 248-257.

# Appendix A

# COMSOL 4.1 Theory

The piezoelectric effect couples the electrostatic and mechanical domains, so the methods of finite-element approximations of such systems are different from regular finite-element procedures. In COMSOL 4.1, material data for piezoelectric devices are defined in much the same way as other materials, but with the addition of changes in convention and piezoelectric coefficient matrices. Instead of the traditional notation order of [xx, yy, zz, xy, xz, yz], the Piezoelectric Devices interface in COMSOL 4.1 uses Voight notation, i.e. [xx, yy, zz, yz, xz, xy], to be consistent with manufacturer data specifications. Most material data comes in the strain-charge form (see Chapter 1, equations 10 and 11), but COMSOL can automatically convert from strain-charge to stress-charge, where T and D are the independent variables.

To incorporate non-piezoelectric materials into the system, the Piezoelectric Devices interface allows options for piezoelectric materials and linear elastic solid materials. The linear elastic model can decouple the material to solve purely structural equations. Material data is entered for the elasticity matrix in the standard notation order, so the ordering is different from the piezoelectric elasticity matrix. Initial stress, strain and electric displacement are added directly to the constitutive relationships,

e.g. T becomes $T-T_0$ for initial prestress.

Initial prestress induces strains that violate the small deformation approximations used to validate linear piezoelectric equations. To account for large deformations and geometric nonlinearities due to prestress, Green strains are used, as they reference undeformed geometry. The electrical displacement is replaced by an expression for electric polarization change due to stress/strain. The constitutive equations are then modified to:

$$T_i = c_{ij}^E * S_j + e_{ik}^T * E_k \tag{21}$$

$$P_m = e_{mj} * S_j + (\epsilon_0 \epsilon_{mn} - \epsilon I) * E_n \tag{22}$$

Then the electric displacement is calculated using the following relation:

$$D_m = P_m + \epsilon_0 J C^{-1} E_n \tag{23}$$

C is the right Cauchy-Green tensor $C= F^T F$, and J is the determinant of F [25].